



## In situ investigation of rapid subsurface flow: Temporal dynamics and catchment-scale implication

Lisa Angermann<sup>1</sup>, Conrad Jackisch<sup>2</sup>, Niklas Allroggen<sup>3</sup>, Matthias Sprenger<sup>4,5</sup>, Erwin Zehe<sup>2</sup>, Jens Tronicke<sup>3</sup>, Markus Weiler<sup>4</sup>, and Theresa Blume<sup>1</sup>

<sup>1</sup>Helmholtz Centre Potsdam, GFZ German Research Centre for Geosciences, Section Hydrology, Potsdam, Germany

<sup>2</sup>Karlsruhe Institute of Technology (KIT), Institute for Water and River Basin Management, Chair of Hydrology, Karlsruhe, Germany

<sup>3</sup>University of Potsdam, Institute of Earth and Environmental Science, Potsdam, Germany

<sup>4</sup>University of Freiburg, Institute of Geo- and Environmental Natural Sciences, Chair of Hydrology, Freiburg, Germany

<sup>5</sup>University of Aberdeen, School of Geosciences, Geography & Environment, Aberdeen, Scotland, UK

*Correspondence to:* Lisa Angermann (science@lisa-angermann.de)

### Abstract.

Preferential flow is omnipresent in natural systems. It links multiple scales from single pores to entire hillslopes and potentially influences the discharge dynamics of a catchment. However, there is still a lack of appropriate monitoring techniques and thus, process understanding. In this study, a promising combination of 2D time-lapse ground-penetrating radar (GPR) and soil moisture monitoring was used to observe preferential flow processes in highly structured soils during a hillslope-scale irrigation experiment. The 2D time-lapse GPR data were interpreted using structural similarity attributes, highlighting changes between individual time-lapse measurements. These changes are related to soil moisture variations in the subsurface. In combination with direct measurements of soil moisture, the spatial and temporal characteristics of the resulting patterns can give evidence about subsurface flow processes. The response dynamics at the hillslope were compared to the runoff response behavior of the headwater catchment. The experiment revealed a fast establishment of hillslope-scale connectivity despite unsaturated conditions, with high response velocities of up to  $10^{-3} \text{ m s}^{-1}$  or faster, and a high portion of mobile water. These processes substantially impact the overall catchment response behavior. While the presented approach is a good way to observe the temporal dynamics and general patterns, the spatial characteristics of small-scale preferential flow path could not be fully resolved.



## 1 Introduction

### 1.1 Methodological challenge of preferential flow

Preferential flow or rapid subsurface storm flow is omnipresent in hydrology (Uhlenbrook, 2006) and today accepted as being the rule rather than the exception (Flury et al., 1994). The specific challenge of investigating preferential flow lies in its manifestation across scales, its high spatial variability, and pronounced temporal dynamics. A considerable number of experimental and model approaches have been proposed to investigate the issue (Beven and Germann, 1982; Šimůnek et al., 2003; Gerke, 2006; Weiler and McDonnell, 2007; Köhne et al., 2009; Beven and Germann, 2013; Germann, 2014). However, rapid flow in structured soils is still a challenge to current means of observation techniques, process understanding and modeling.

At the plot-scale the focus is generally on vertical flow in discrete pores and structures. These flow processes are investigated in irrigation experiments with dye, salt and isotopic tracers or combinations of those (e.g. Germann, 2014; Van Schaik et al., 2014; Jackisch et al., this issue) as well as experiments with neutron radiographs at even smaller scales (Hincapié and Germann, 2010; Snehota et al., 2015).

In previous studies at the hillslope-scale, the focus often is on lateral flow processes and the establishment of overall connectivity. Hillslope-scale excavations yield information on spatial extent and characteristics of preferential flow paths in 3D (Anderson et al., 2008; Graham et al., 2010), but are highly destructive and lack the temporal component. Hillslope-scale tracer experiments in contrast, resolve temporal dynamics and velocities (Wienhofer et al., 2009; McGuire and McDonnell, 2010), but lack the spatial information. Hillslope-scale experiments are usually very labor intensive and require high technical effort and most studies are concentrated on well-monitored trenches (McGlynn et al., 2002; Tromp-Van Meerveld and McDonnell, 2006; Vogel et al., 2010; Zhao et al., 2013; Bachmair and Weiler, 2012). Blume and van Meerveld (2015) give a thorough review of investigation techniques for subsurface connectivity and find experimental studies on this topic underrepresented in hydrological field research.

In recent years, a trend towards non-invasive methods for hillslope-scale observations emerged (Gerke et al., 2010), which has been an important improvement with regard to repeatability and spatial and temporal flexibility of observations (Beven and Germann, 2013). In this context various geophysical methods have been applied for subsurface exploration (e.g. Wenninger et al., 2008; Garré et al., 2013; Hübner et al., 2014). From all geophysical techniques ground-penetrating radar (GPR) is known as the tool providing the highest spatial resolution. At minimal invasive cost it provides information on subsurface structures in electrically resistive soils (e.g. Lambot et al., 2008; Bradford et al., 2009; Jol, 2009; Schmelzbach et al., 2011, 2012; Steelman et al., 2012). Its short measurement times and high sensitivity towards soil moisture predestine GPR for monitoring subsurface flow. Nevertheless, only few field studies exist which successfully applied surface based GPR for the investigation of subsurface flow paths (Truss et al., 2007; Haarder et al., 2011; Guo et al., 2014; Allroggen et al., 2015b).

These studies identified time shifts and amplitude variations along manually selected reflection horizons, which give evidence on vertical infiltration. Allroggen and Tronicke (2015) suggest a novel data analysis procedure for GPR data based on an attribute analysis of 2D time-lapse GPR transects. The attributes highlight specific areas of increased difference which are



interpreted as local changes in soil moisture and thus related to subsurface flow paths. This method opens new perspectives for the investigation of preferential flow at the hillslope-scale.

At the basin-scale, preferential flow is treated as an intrinsic property of the investigated system. Most experimental evidence stems from analyses of the dynamic water balance (McGuire and McDonnell, 2010), salt tracers (Sheng et al., 2014) and stable isotopes (Gazis and Feng, 2004; Peralta-Tapia et al., 2014). The focus of these studies is on transit time distributions or the identification of source areas and storages throughout the catchment. Both are indicative of the spatial organization of the landscape and skewed or even multi-modal transit time distributions suggest preferential flow processes. Hydrological dynamics of different observations throughout the catchment were correlated to empirically relate catchment response to hillslope processes (Bachmair and Weiler, 2014). However, it is difficult to draw conclusions on relevant hillslope processes based on catchment-scale observations and most studies employ models to verify their hypotheses on relevant processes (e.g. Fenicia et al., 2014).

A particularly distinct example of a multi-modal transit time distribution is a double-peak hydrograph. These hydrographs are observed in many different catchments and have been subject to a number of research projects (e.g. Onda et al., 2001; Wenninger et al., 2004; Zillgens et al., 2007; Graeff et al., 2009; Wrede et al., 2015). They are characterized by an almost instant response with steep rising and declining limbs, and a second prolonged response with a delay of several hours or even days after the onset of precipitation. In the literature, the first peak is often attributed to surface runoff or an immediate reaction of the riparian zone. The reasons for the second peak are often subsumed under the vague term *subsurface flow processes*, which summarizes a wide variety of different processes.

The specific characteristics of subsurface flow processes are a crucial component in the hydrological behavior of a landscape. Understanding the process of the establishment of flow paths from the plot- to hillslope-scale on the one hand, and the relation between hillslope processes and catchment-scale dynamics on the other, is a major step towards understanding runoff generation mechanisms and the functional organization of catchments (Zehe et al., 2014).

## 1.2 Objectives and experimental approach

To fully understand the role of preferential flow it is necessary to use a multi-scale approach. Methods are required which are capable of covering both, spatial patterns and temporal dynamics at multiple scales. The combination of conventional hydrological methods and spatially and temporally flexible, non-invasive geophysical measurements has the potential to meet these requirements. We thus propose time-lapse GPR measurements as an alternative to established methods like trenches or dye tracer excavations.

In this study, we aimed at identifying and monitoring preferential flow processes across scales. The central element of the experimental work was a hillslope-scale irrigation experiment, which was specifically designed to observe both, vertical and lateral flow processes. Monitoring entailed a combination of soil moisture observations and 2D time-lapse GPR measurements. The experiment was complemented by plot-scale tracer experiments, a structural survey, a basic hydrograph analysis and stable isotope sampling.



- This article is the first part of the companion paper and focuses on the temporal dynamics of preferential flow. We compared the identified processes and dynamics with the hydrological response behavior to a natural summer storm event to evaluate their catchment-scale relevance. The potential of the methods for the investigation of subsurface flow processes at the hillslope-scale and the characterization of typical runoff generation mechanisms are discussed and possible further improvements suggested.
- 5 To complement the temporal perspective on preferential flow, the second part by Jackisch et al. (this issue) concentrates on its spatial characteristics from the plot- to hillslope-scale in relation to subsurface structures.



## 2 Methods

### 2.1 Study site

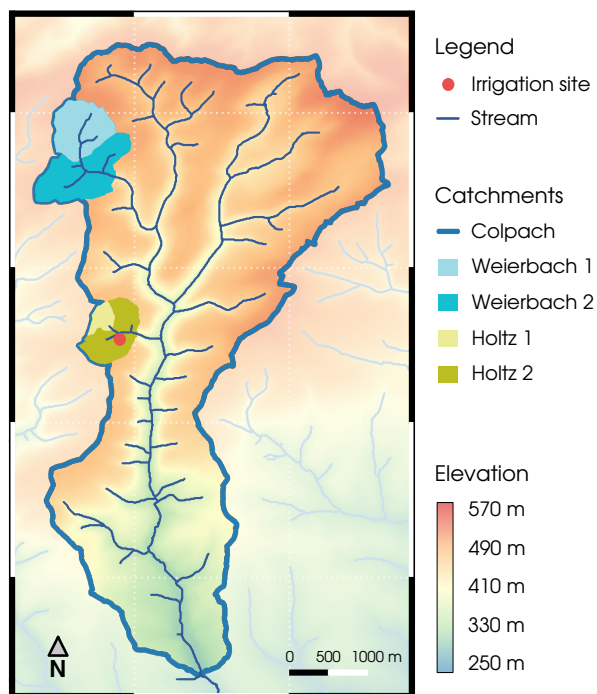


**Figure 1.** Map of the investigated Colpach River catchment and the four gauged sub-catchments. The site of the hillslope-scale irrigation experiment is located in the Holtz 2 catchment and indicated in red.

The investigated area is located at the south eastern edge of the Ardennes Massif in western Luxembourg. It consists of a number of nested sub-catchments of the Colpach River catchment, which is part of the Attert River basin. The landscape of this area is characterized by Devonian schist bedrock (Colbach and Maquil, 2003). The soils are young and composed of eolian loess deposits and weathered schist debris. Under periglacial conditions, the weathered rocks were relocated by solifluction, causing an often horizontal or slope parallel orientation of the saprolite (Juilleret et al., 2011). The periglacial deposit layer (basal layer) is overlain by shallow top soil (upper layer). The soil is classified as Haplic Cambisol (CM, IUSS Working Group WRB (2006)).

The schist bedrock below is strongly inclined with almost vertical foliation and considered relatively impermeable but with fractures which can function as a complex flow network with local storage in the rock cracks when saturated (Van den Bos et al., 2006; Kavetski et al., 2011). The subsurface structures are of predominately geogenic origin and considered temporally persistent.



Within this landscape, a typical hillslope consists of agriculturally used elevated plateaus and forested valleys with relatively steep slopes (15° to 25°). While the headwater catchments of the investigated area are usually narrow with marginal floodplains, the main Colpach River network is characterized by wider valleys with more pronounced floodplains.

The average annual precipitation between 2011 and 2014 was 965 mm, the annual average air temperature was 8.8 °C. These data stem from a meteorological station from ASTA (*administration des services techniques de l'agriculture de Luxembourg*) close to Roodt.

The experimental work conducted in the frame of this study focused on a north facing hillslope in the Holtz headwater catchment. The experiment was supplemented by hydrological data from five neighboring headwater catchments of different size. All sub-catchments as well as the location of the irrigation site are shown in Fig. 1.

## 10 2.2 Hydrological response monitoring

The hydrological response behavior of several nested sub-catchments was investigated. At four locations v-notch or trapezoidal gauges were installed and equipped with CTD sensors (Decagon Devices Inc.). Water levels were measured every 15 min. Precipitation was monitored with tipping buckets (Davis Instruments Corp.) in the Holtz 1 headwater. All data were logged with CR1000 data loggers (Campbell Scientific Inc.).

At the same locations and additionally close to the source of the Holtz River (Holtz 1 in Fig. 1), water samples were taken with auto samplers (ISCO 3700, Teledyne). The bottles of the auto samplers were pre-filled with styrofoam beads to avoid evaporation from the sample bottles. Samples were then transferred to glass bottles and analyzed in the laboratory at the Chair of Hydrology, University of Freiburg. The isotopic composition ( $^{18}O$  and  $^2H$ ) of the water samples was measured with a wavelength-scanned cavity ring-down spectrometer (Picarro L2120-iWS-CRDS). The results are given in the  $\delta$ -notation in [%o], describing the deviation of the ratio between heavy and light isotopes ( $^{18}O/^{16}O$ ) relative to the ratio of the Vienna Standard Mean Ocean Water (VSMOW).

In addition to the stream water, rainfall water was sampled on event basis. The water from the saturated zone was manually sampled monthly from piezometers close to the gauges using a pump.

To calculate the event water contribution, we applied a simple mixing model (Pearce et al., 1986). Equation 1 shows the calculation of the discharge attributed to the natural rain event  $Q_e$ , based on the isotopic composition of the base flow ( $c_b$ ) three days before the storm event, the river water during and after the event ( $c_t$ ), and the rain water ( $c_e$ ) (Leibundgut et al., 2011).  $Q_t$  is the total discharge during and after the event, which is constituted of the two components  $Q_e$  and  $Q_b$ , i.e. event water and pre-event water.

$$Q_e = Q_t \cdot \frac{c_t - c_b}{c_e - c_b} \quad (1)$$



## 2.3 Hillslope-scale irrigation experiment

### 2.3.1 Irrigation setup

The plot of the hillslope-scale irrigation experiment is located on the lower section of the investigated hillslope and has a slope of  $\sim 14^\circ$ . While vegetation at the hillslope is dominated by beech forest (*fagus sylvatica*) of mixed age, the irrigation plot is placed in an area with no major trees. Except for few young trees with breast height diameters below 0.1 m in the downhill monitoring area, all shrubs were cut to facilitate GPR measurements and allow for uniform irrigation. The entire investigated hillslope section covers an area of approximately 260 m<sup>2</sup>.

The irrigation setup is shown in Fig. 2. Four circular irrigation sprinklers (Wobbler, Senninger Irrigation Inc.) were arranged in a 5 m by 5 m square in the upper part of the experimental site. This 25 m<sup>2</sup> area spanned by the sprinklers is referred to as the core area with relatively homogeneous irrigation intensity of  $\sim 30.8 \text{ mm h}^{-1}$  over 4.5 h. Total water input at the core area was 141 mm. These settings aimed at activating all potential flow paths, rather than mimicking natural conditions, and were chosen on basis of an *a priori* simulation of the experiment.

The surrounding area functioned as buffer of about 4 m with less intense irrigation, thus mitigating boundary effects. A rain shield defined the lower boundary of the core area as a sharp transition to the non-irrigated area below. The water from the rain shield was collected with a gutter and routed away from the investigated area. The overall irrigation area (including core area and buffer) covered  $\sim 120 \text{ m}^2$ .

To monitor the irrigation we used a flow meter at the main water supply of the irrigation system to measure the absolute water input. Furthermore, one tipping bucket was used to quantify the temporal variability of applied irrigation, and 42 mini rain collectors, evenly distributed across the core area, covered the spatial homogeneity of the irrigation intensity. The topography of the experimental site, as well as all devices and installations were mapped with a total station (Leica Geosystems AG).

The experiment took place on June 21st, 2013. After one week of dry weather, two natural rainfall events of 18 mm and 25 mm had occurred on June 20th,  $\sim 20 \text{ h}$  before the experiment.

### 2.3.2 Process monitoring

The monitoring of hydrological processes during and after the irrigation period was accomplished with a combination of methods: A dense array of soil moisture profiles for time domain reflectometric (TDR) measurements, and four GPR transects located downhill of the core area and oriented parallel to the rain shield for time-lapsed GPR measurements. The latter yielded vertical cross sections of the subsurface.

A surface runoff collector was installed across 2 m at the lower boundary of the core area. Surface runoff was collected by a plastic sheet installed approximately 1 cm below the interface between litter layer and the Ah horizon of the soil profile and routed to a tipping bucket.

An array of 16 access tubes for soil moisture measurement with TDR probes (Pico IPH, IMKO GmbH) covered the depth down to 1.7 m below ground. The layout consisted of three diverging transects with four TDR profiles in the lower half of the core area, the highest density of profiles just downslope of the rain shield, and the furthest profile about 9 m downhill (Fig. 2B).

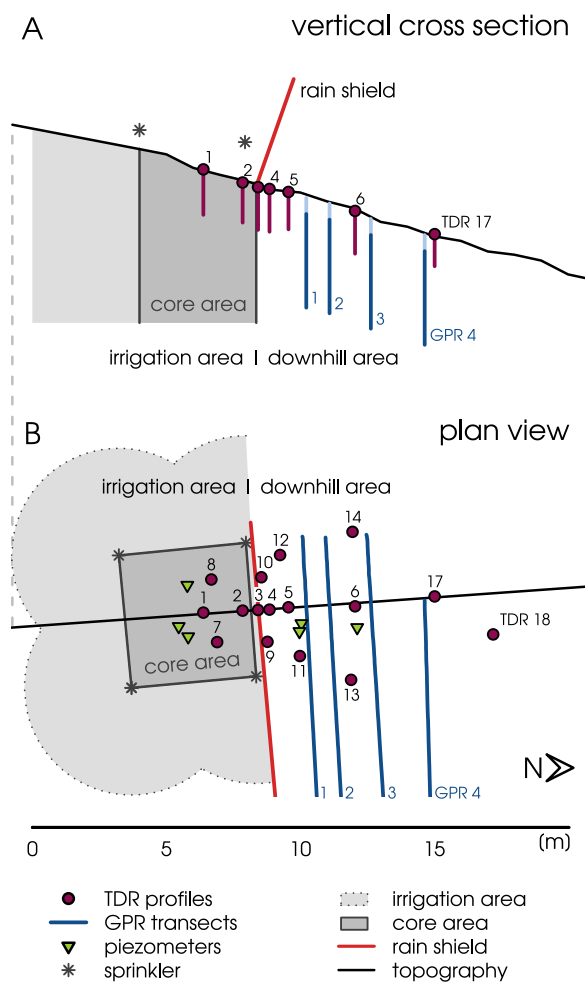


**Figure 2.** Vertical cross section (A) and plan view (B) of the experimental setup and sprinkler array. Location and depth of the TDR profiles and GPR transects are given in purple and blue, respectively. The black line in B marks the vertical cross section depicted in A.

This setup allows for the separate observation of predominately vertical flow at the core area and lateral flow processes at the downhill monitoring area.

Two versions of the TDR sensor were employed, with either 0.12 m or 0.18 m integration depth. These sensors were lowered to different depths in the access tubes, where they measured the dielectric permittivity of the surrounding soil in the time domain. Given a mean penetration depth of 5.5 cm and a tube diameter of 4.2 cm this yields an integration volume of  $\sim 0.72$  L and 1.05 L, respectively. The three TDR probes were used to take manual measurements following a flexible measuring routine to cover active soil profiles with higher frequency. Measurements were conducted in 0.1 m depth increments.



The monitoring setup also included a transect of 6 piezometers equipped with CTD loggers (Decagon Devices Inc.). The piezometers were installed in depths between 1 m and 2 m. Because none of them showed a properly detectable reaction they are not taken into consideration in this study.

In addition to the hydrological methods, GPR was used to monitor the shallow subsurface. 2D time-lapse GPR measurements were conducted along four transects across the downhill monitoring area. The transects had distances of ~2 m, 3 m, 5 m and 7 m to the lower boundary of the core area and were arranged approximately perpendicular to the topographic gradient. Each transect was measured nine times. One measurement was taken before irrigation started and the last one about ~24 h after irrigation.

The GPR system consisted of a pulseEKKO PRO acquisition unit (Sensors and Software Inc.) equipped with shielded 250 MHz antennas. The data were recorded using a constant offset of 0.38 m, a sampling interval of 0.2 ns and a time-window of 250 ns. For accurate positioning, a kinematic survey strategy was employed. The survey was based on a self-tracking total station (Leica Geosystems AG), which recorded the antenna coordinates as described by Boeniger and Tronicke (2010). To guarantee the repeatability of the 2D time-lapse GPR measurements, all four transects were defined by wooden guides for an exact repositioning of the antennas. The measurement of one transect took approximately 2 min and measurements of all four transects were taken roughly every 1.5 h during and after irrigation as well as 12 h and 24 h after irrigation ended.

## 2.4 Data analysis

### 2.4.1 TDR data analysis

Almost 5000 individual soil moisture measurements were taken during the irrigation experiment. As the three TDR probes had different integration depths (0.12 m and 0.18 m), the measurements had a different depth offset relative to the ground surface (0.08 m and 0.12 m, referenced to the center of the probe) and had to be aligned. To do so, the measurements, which were originally taken in 0.1 m increments, were resampled in depths by linear interpolation. Due to the potentially short correlation length of soil moisture (Zehe et al., 2010), inverse distance interpolation between two locations is generally not appropriate. In case the vertical profiles, however, the integration depths of the probes exceeded the measuring increments. Due to the resulting overlap of the integration volumes, this procedure was assumed to be adequate. The measurement of one depth increment took approximately between 10 s to 30 s.

All TDR measurements were referenced to the last measurement before irrigation. The resulting data set of relative soil moisture changes  $\Delta\theta$  was used for the discussion of soil moisture dynamics, velocity calculation (Sec. 2.4.3), and comparison with the time-lapse GPR data. The storage changes in the top 1.4 m of the core area were estimated based on the 4 TDR profiles. Together with the time series of water input this data was used to estimate the mass balance dynamics of the core area.

### 2.4.2 2D time-lapse GPR measurements

The time-lapse GPR survey comprised repeated recordings of vertical 2D GPR data along the four transects. The data processing of each measurement relied on a standard processing scheme, including bandpass filtering, zero time correction, exponential



amplitude preserving scaling, inline fk-filtering, and a topographic migration approach, similar to the procedure presented by Allroggen et al. (2015a). The GPR data were analyzed using an appropriate constant velocity and gridded to a 2D transect with a regular trace-spacing of 0.02 m.

There is no standard interpretation procedure for the analysis of time-lapse GPR data. Most approaches are based on calculating trace-to-trace differences (Birken and Versteeg, 2000; Trinks et al., 2001) or picking and comparing selected reflection events in the individual time-lapse transects (Allroggen et al., 2015b; Haarder et al., 2011; Truss et al., 2007). In the context of this study, however, both approaches provided only limited interpretable information. Considering the methodological uncertainty, the highly heterogeneous soil did not provide reflectors which were a suitable reference. Therefore, we used a time-lapse structural similarity attribute presented by Allroggen and Tronicke (2015), which is based on the structural similarity index known from image processing (Wang et al., 2004). This approach incorporates a correlation-based attribute for highlighting differences between individual GPR transects and has been shown to improve imaging, especially for noise data and limited survey repeatability.

The calculated structural similarity attributes are a qualitative indicator for relative deviations from the reference state. The GPR data suggested remaining mobile water from the natural rain event when the experiment was started. Therefore, the last acquisition time approximately 24 h after irrigation start was chosen as the reference time for all GPR transects. Based on the assumption, that the reference state is the one with the lowest water content, decreasing structural similarity was interpreted as an increase in soil moisture.

For converting GPR two-way travel time (TWT) into depth, we used the average measured GPR propagation velocity of  $0.07 \text{ m ns}^{-1}$ . This velocity is based on additional common midpoint data and the assumption of static conditions during the experiment. Using this velocity, the GPR transects covered a TWT of 120 ns, which corresponds to a depth of  $\sim 4.2 \text{ m}$  below ground surface. Approximately the first 20 ns of each transect are influenced by the interfering arrival of the direct wave and the ground wave. Consequently, we observe no interpretable reflected energy in the uppermost time window. Thus, the 2D GPR measurements imaged the subsurface between approximately 0.7 m to 4.2 m depth below ground.

To interpret the structural similarity attribute images, we discriminated between the signal of the natural rain event and the irrigation. Signals in the first two measurements (i.e. approximately 6.5 h before and immediately at irrigation start) were attributed to the natural rain event. Once the structural similarity attribute value of a pixel decreased more than 0.15 afterwards, the signal of that pixel was attributed to the irrigation. The same procedure was applied to infer the time of first response to the irrigation signal, which was used to calculate response velocities.

### 2.4.3 Response velocity calculation

As no tracers were used for irrigation, dynamic processes had to be inferred from changes in state. For TDR measurements, the time of first response was defined as an increase of soil moisture of 2 vol% relative to initial conditions. The time of first response was identified for each TDR profile and depth increment.



Due to the experimental setup, soil moisture dynamics on the core area were dominated by vertical processes, while lateral processes controlled the dynamics at the downhill monitoring area. Accordingly, vertical and lateral response velocities were calculated from core area and downhill monitoring area TDR profiles, respectively.

As a continuous wetting of the soil profile could not be assumed, all velocities were calculated for the entire depth (or distance) instead of depth increments. Velocities are therefore not valid for the depth increment they were calculated for, but are integrated values describing processes in the entire soil column above. This procedure accounts for heterogeneous processes and preferential flow paths, which may bypass shallower depths without leaving a detectable soil moisture signal.

Lateral velocities account for the depth and distance between the rain shield and TDR profile and therefore, integrate lateral and vertical flow. They were calculated for every depth of the soil moisture profiles at the downhill monitoring area. The time of the very first response signal measured on the core area was used as reference time  $t_0$ , which was 15 min after irrigation start. Due to the slope-parallel or horizontal orientation of the saprolite, we assumed that the water flows either vertically or laterally rather than diagonally. Based on this assumption, the distances were calculated from the slope parallel distance of each profile from the lower boundary of the core area plus the depth of every measuring point. The distance assumptions for both, vertical and lateral velocity calculations, do not resolve tortuosity of flow paths and therefore, drastically reduce the complexity of the flow path network to its integral behavior. The calculated velocities are thus not to be interpreted as *in situ* flow velocities in the flow paths, but rather as the minimum necessary velocity explaining the observed arrival of the wetting signal.

The same holds true for the lateral velocities calculated from GPR data. Concordant to the separation of the natural rain event signal and the irrigation signal, the first decrease in structural similarity of more than 0.15 was interpreted as the arrival of the irrigation signal. Single structures and flow paths are not the focus of this article and will be discussed by Jackisch et al. (this issue). Here, we therefore simplified the 2D patterns to a depth distribution of occurring velocities. To do so, all areas activated during one measurement were accumulated by depth, and given as portion of the entire width of each GPR transect. Comparable to the procedure applied to the TDR data, the response velocities were then calculated from the respective measuring time, the distance between transect and irrigation area and the depth. The resulting patterns show the spatial portions of the depth increment which are connected to flow paths of the calculated velocity or faster and give an idea about the spatial distribution of the GPR response velocities.



### 3 Results

#### 3.1 Catchment response to natural rainfall events

The catchment response of the investigated headwater catchments showed a strong seasonality. During winter, direct and flashy runoff reactions prevailed. In the vegetated season the pattern reversed to low base flow and relatively weak reactions to rain events. Even during this time, however, strong storm events triggered double-peak runoff responses, demonstrating the effect of a bimodal transit time distribution through the catchment. Figure 3 pictures the hydrologic response of the gauged sub-catchments to the summer storm event just before the hillslope-scale irrigation experiment with typical double-peak hydrographs. In the headwater catchments (Holtz 2, Weierbach 1 and 2), the first peak occurred almost instantly, while the Colpach main stem showed a delay of approximately 3 h. The second response was prolonged and peaked approximately 36 h after the event. The strength and ratio of the two peaks varied across different sub-catchments and according to hydrological conditions, but the general pattern is characteristic for the hydrological behavior of the Colpach River catchment. Similar behavior was also reported by Fenicia et al. (2014) and Wrede et al. (2015), whose investigations focused on the Weierbach 1 catchment.

A simple mass balance calculation revealed, that the first peak constituted 7.5 % of the total event runoff at gauge Holtz 2. The total event runoff coefficient was 0.44. Referenced to the precipitation amount, about 3.3 % of the input left the headwater within 7 h after the rain event. In the neighboring Weierbach catchment and the Colpach main stem, the first peak contributed more strongly to the total event runoff (14.2 % and 12.9 % at Weierbach 1 and 2, and 19.7 % at Colpach).

The  $\delta^{18}O$  signature of the stream water is indicative for the origin of the water. It showed strong dynamics during the discharge response to the rain events on June 20 (Fig. 3). The results of the mixing model show that the event water contributed up to 67.6 % of the event runoff during the response to the first rain event in the morning of June 20 (Colpach main stem, 6:00h). After that, the total discharge dropped again, with the event water contribution decreasing to 31.6 %. With the onset of the first peak caused by the major rain event at 19:20h, the event water contribution increased again and reached values of over 50 % (52.4 % in the Colpach main stem at 22:00h, 50.8 % in the Holtz 1 catchment, 21:51h on June 20. Fig. 3). The  $\delta^{18}O$  signature then dropped, indicating event water contributions of around 20 % (22.4 % at 4:00h in the Colpach main stem, 16.6 % at 13:03h in Holtz 2 and 15.0 % at 21:28h in Holtz 2 on June 21). Weierbach 1 and 2 showed the same pattern, with event water contributions of up to 50.0 % for the first peak of the major storm event. This analysis suggests, that the water of the observed rain events quickly entered the river, causing the first immediate reaction, while the second, prolonged peak was mainly fed from pre-event water.

#### 3.2 Hillslope-scale irrigation experiment

##### 3.2.1 Core area water balance

The total irrigation amount on the core area was 141 mm in 4.5 h. The intensity was relatively constant over time, with only weak fluctuations due to gradual clogging of the intake filter. The spatial distribution of the irrigation intensity on the core area was influenced by the sprinkler setup and the slope of the experimental site. The mean intensity on the core area was

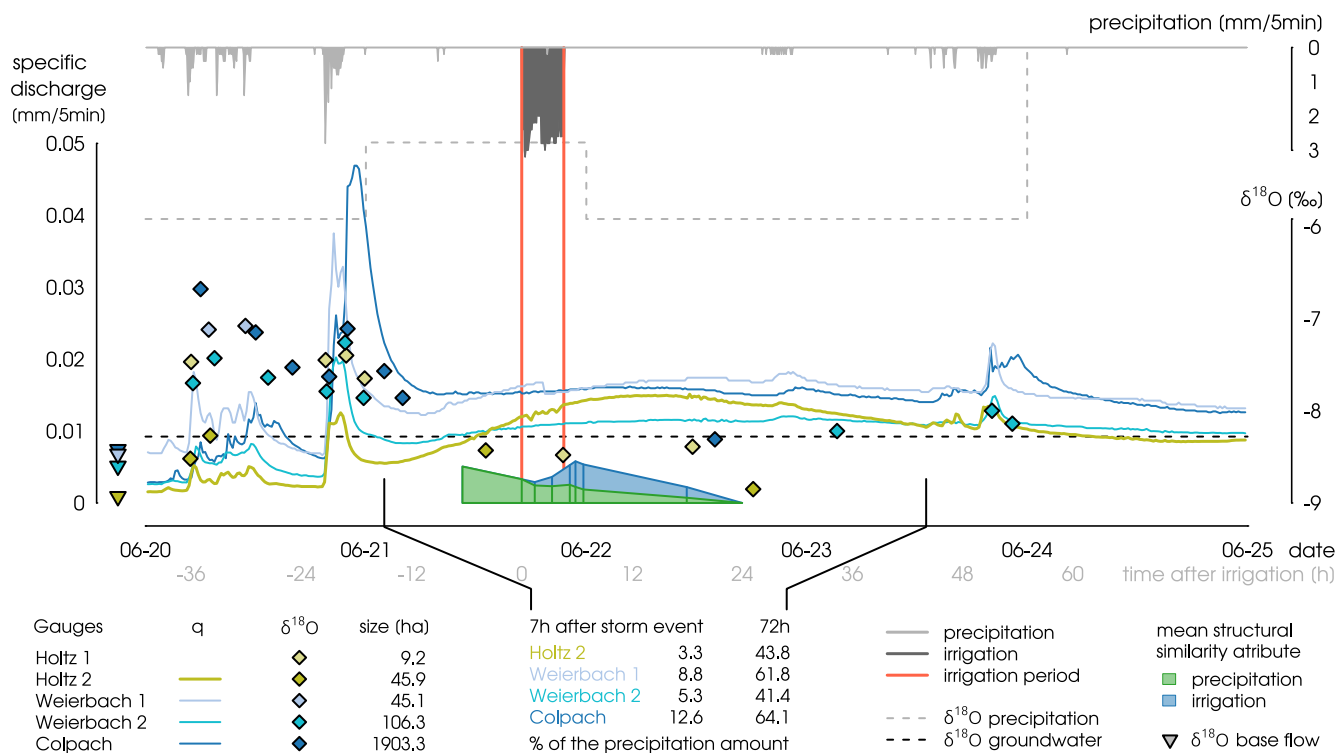


**Figure 3.** The figure shows the natural storm event on June 20, 2013 in the Colpach River catchment and the local intensity of the irrigation on June 21, 2013. The hydrographs below show the discharge response of four nested catchments (solid lines), in combination with the dynamics of the  $\delta^{18}O$  isotopic composition of the surface water (dots). The isotopic composition of the groundwater (annual mean) and the precipitation (daily values) are given by the dashed lines. Furthermore, the dynamic response of the GPR signal to natural and artificial rainfall is given in green and blue. While the first minor rain events caused only weak response, the main event (20 mm) starting at 19:20h caused a double-peak discharge response in all sub-catchments. The irrigation experiment took place approximately 20 h after the rain event.

$38 \pm 9 \text{ mm h}^{-1}$ , with slightly higher values in the vicinity of the four sprinklers. Surface runoff at the lower boundary of the core area started 20 min after irrigation start and amounted to 0.5 L with a relatively constant rate. This equals 0.02 % of the water balance.

The core area mass balance is shown in Fig. 4, depicting the storage increase in the top 1.4 m of the soil. All profiles showed an overshoot in calculated mass recovery in the first 60 min of the irrigation period. In profiles TDR1, TDR2 and TDR8 mass recovery then decreased and dropped below 100 %, while TDR7 increased further, with a maximum overshoot of almost 50 % approximately 2 h after irrigation start. The last measurement during irrigation was taken approximately 50 min before the end of the irrigation period. At this time, the average storage deficit was more than 20 % of the input mass.



The first measurement after irrigation (10 min after irrigation stopped) showed a mean deficit of 50 %. After this fast instantaneous reaction, the water content decreased equably. Mean total mass recovery dropped to 8.9 % after 18.4 h after irrigation start and returned to similar to initial conditions (1.6 %) after 24 h after irrigation start.

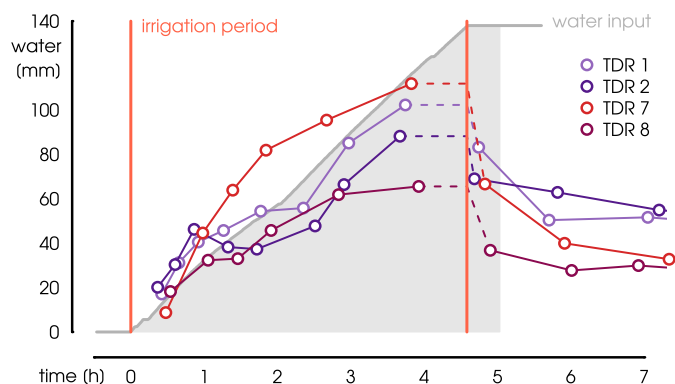


**Figure 4.** Water balance of the top 1.4 m of the soil column for the four core area TDR profiles. Dashed lines indicate the storage increase at the last measurement before irrigation ended.

### 3.2.2 Soil moisture dynamics

5 The high variability in soil moisture dynamics observed in the TDR profiles is summarized in Fig. 5. The four uppermost panels (row 1 and 2) show the core area profiles. Columns represent the three diverging TDR transects. The general pattern observed at the core area was characterized by strong and comparably fast response in the top 0.4 m of the soil, and below the depths of approximately 1.2 m. The response in between these active layers was more diverse and generally weaker.

Soil moisture in the top 0.4 m of the soil of TDR1, TDR7 and TDR8 quickly stabilized around constant values, indicating the establishment of quasi steady-state conditions. After the end of the irrigation, the soil moisture quickly declined down to a  $\Delta\theta$  of 4 vol%, indicating a very fast response to the dynamics of the water input. In contrast to the fast establishment of steady-state conditions and the fast decline, a slightly increased water content of up to 4 vol% above initial conditions was persistent in distinct depth increments and was also measured even 24 h after irrigation stopped.

The soil moisture patterns at the downhill monitoring area were more diverse. Profiles located directly below the rain shield (TDR9, TDR3 and TDR10 with a distance to core area of 0.2 m to 0.5 m, Fig. 5) exhibited dynamics that resemble the reaction at the core area, but with mostly lower intensities and higher variability in depth. More distant TDR profiles however, showed a highly variable picture. Distinct layers in variable depths were activated, while no change of the water content was seen in the other soil depths. Especially noteworthy are TDR10 and TDR11, which showed a strong soil moisture increase of up to 18 vol% below 1.4 m depth and around 10 vol% in the top 0.3 m of the soil. Profiles TDR13, TDR6 and TDR14 showed only weak signals, with the strongest response below 1.4 m below ground in TDR6. While the results from the left (TDR7, TDR9 and TDR11) and the right transect (TDR8, TDR10 and TDR12, see Fig. 5) suggested lateral flow in different depths, the central



transect (TDR1 through TDR6) did not indicate lateral flow. This might either be due to a divergent flow field or due to tortuous flow path.

### 3.2.3 2D time-lapse GPR

The TDR measurements at the downhill monitoring area were complemented by the 2D time-lapse GPR measurements (see Fig. 2), yielding 2D images of structural similarity attributes referenced to the last measurement. Changes of structural similarity attributes are interpreted as changes in soil moisture, showing qualitative information about the spatial patterns of flow paths and their temporal dynamics. The structural similarity attribute information from all GPR transects are plotted in Fig. 6.

The high initial signals (i.e. localized low structural similarity to the reference measurement 24 h after irrigation start) in all transects and their decrease during the first measurements until 1.5 h after irrigation start indicated water remaining from the preceding natural rain event. While transect 1 showed only a weak signal of the natural event in the first measurement, transects 2 and 3 exhibited stronger and longer lasting signals.

The natural rain signal disappeared or was overpowered by the irrigation signal at 20:30h, which is 3.3 h after irrigation start and about 24 h after the natural rain event. The generally low dynamics in transect 4 were due to its proximity to the floodplain and therefore generally wetter conditions and less capacity for additional wetting.

The signal caused by the irrigation water is shown in blue in Fig. 6. The first weak irrigation signals appeared in the first measurement after irrigation start (1.5 h), with transect 1 showing the clearest response. After about 3 h strong localized signals occurred and increased in intensity over time. The general maximum was reached approximately 5.3 h after irrigation start, showing distinct activated flow paths. Most signals started to slowly decline after 7 h, which is 2.5 h after the end of the irrigation period.

In transect 2 some weak signals appeared in the depth below 2.5 m 1.5 h after irrigation start. At this time, the signal was close to noise level, but the pattern became stronger and more distinct in the following measurements. At transect 3, the persisting signal of the natural rain event made it difficult to identify the irrigation induced response. However, a weak irrigation signal appeared at 1.5 h and reached its maximum at approximately 7 h after irrigation start. At transect 4 the structural similarity attribute values were generally low, which indicates a low deviation from the reference state. Either the mobile water showed relatively low dynamics (with regard to total mass over time), or water was less confined to specific structures and local changes are less pronounced. Both interpretations confirm that this transect was generally wetter due to its proximity to the floodplain. Overall, the experiment does not appear to have affected this transect much.

The overview over all GPR measurements in Fig. 6 visualizes the dynamics of the hillslope section. The green natural rainfall signal faded from uphill to downhill, with the highest intensity and duration in transect 3. After irrigation start, the blue irrigation signal appeared, gradually propagating downhill and eventually overpowering the natural rain signal. 18 h after irrigation start (i.e. approximately 14 h after irrigation ended), all fast dynamics vanished. This suggests steady soil moisture conditions and thus, the absence of highly mobile water in all transects. The mobile water either left the monitored area, or dispersed by diffusion into the matrix surrounding preferential flow paths.

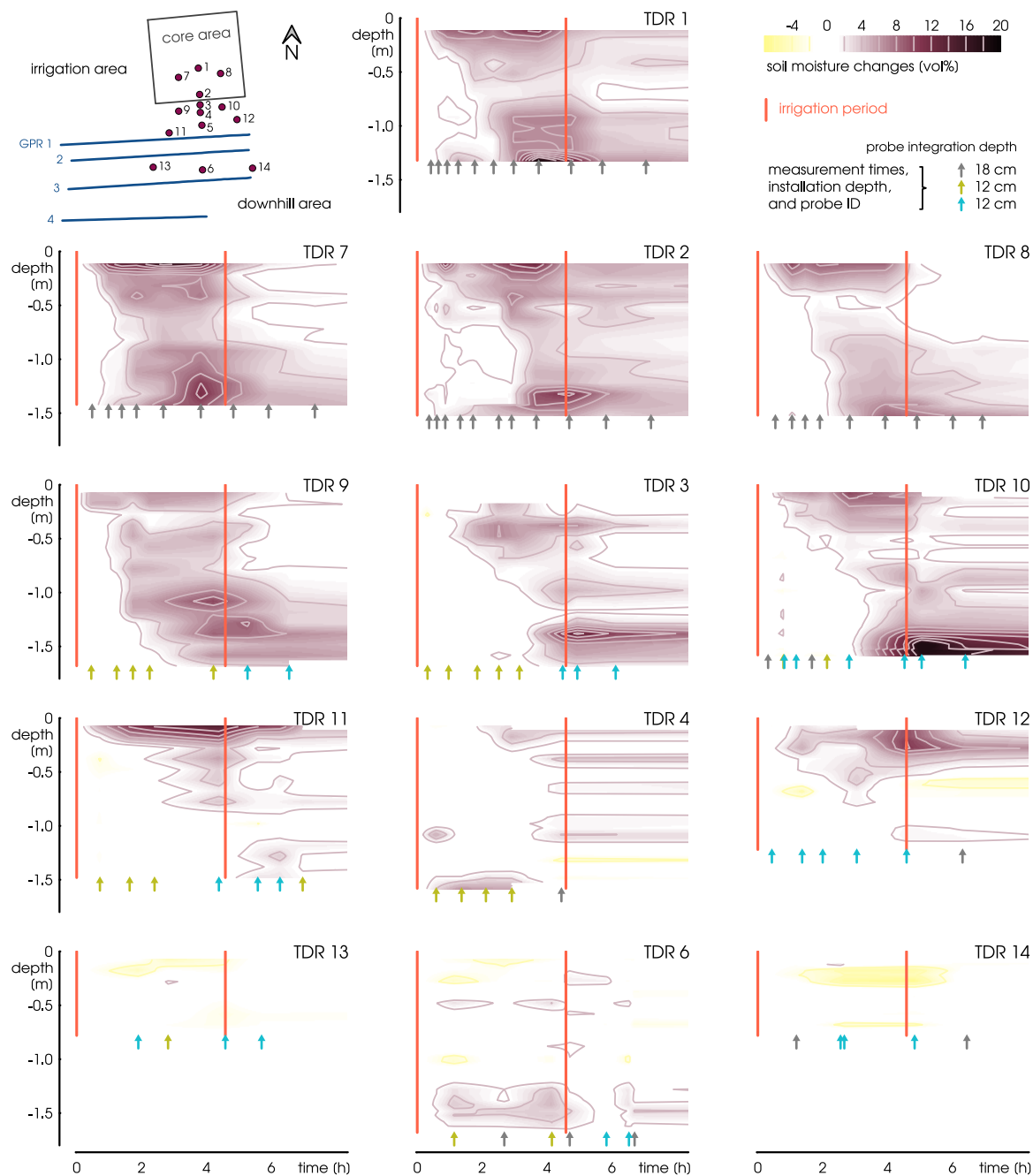


**Figure 5.** The soil moisture data measured at the TDR profiles at the irrigation site, showing the soil moisture dynamics in depth. The top four plots show all four core area profiles, columns are arranged according to the three diverging transects in downhill direction. Rows are approximately at the same contour line. Measurements were taken at 0.1 m increments. While data analysis was based on non-interpolated data, soil moisture measurements were here interpolated linearly for better visualization. The plots cover the time from irrigation start until 9 h after irrigation start to focus on the first soil moisture response. Arrows indicate the measurement times and installation depth of each TDR profile. Time is given in [h] after irrigation start.



Besides the soil moisture dynamics, there were some spatial features revealed by the GPR measurements, which are relevant for understanding hillslope-scale flow processes. Firstly, both, the natural rain event and the irrigation caused advective flow in discrete structures more or less evenly distributed over the hillslope cross-section. An (ephemeral) groundwater body or specific flow layers could not be identified in the top 4.2 m of the subsurface. Secondly, the artificial irrigation had only a minor impact in comparison to the natural rain event, despite higher local input. The accumulated upslope area was therefore more important than irrigation intensity or duration. The heterogeneity and disconnectivity of the preferential flow network and its methodological aspects are discussed separately by Jackisch et al. (this issue).

### 3.2.4 Combination of TDR and GPR measurements

GPR and TDR are both sensitive to the electrical permittivity of the soil and hence, are expected to be well comparable. Nevertheless, a quantitative calibration of GPR data by means of TDR measurements was not possible. Due to the sensitivity of GPR measurements to installations in the soil, we kept a certain distance between the GPR transects and the access tubes and removed the TDR probes from the access tubes during the GPR measurements. Furthermore, the overlap in depth between the methods is small, as the TDR measurements extend from 0 m to maximum 1.7 m, while the GPR measurements extend from approximately 0.7 m to 4.2 m. Last but not least, the GPR signal is influenced by a variety of factors and an unambiguous attribution of soil moisture values is arguable. These methodological aspects, combined with the high observed complexity of subsurface structures and flow paths make a quantitative correlation difficult.

However, a qualitative comparison of the results from both methods is possible, and shows a good agreement in space and time. The results from both methods showed similar soil moisture patterns and the dynamics suggested a continuous propagation of the irrigation signal towards greater depth (Fig. 7). In comparison to the TDR signal covering the top 1.7 m, the GPR irrigation signal was shifted slightly downward, which might have been due to inaccuracies in the GPR pulse velocity estimation, or the mere spatial distance between the two locations.

Comparison of the soil moisture response observed in the three diverging TDR transects with the closest positions along GPR transect 1 (see Fig. 6 for locations) show a correlation between signal strength in both datasets. GPR transect 1 shows a strong signal in the lateral position between 5 m to 7 m and 8 m to 10 m, leaving a gap in the area of the center TDR transect. TDR4, TDR5 and TDR6 are the downhill profiles of the center transect and show weak signals, too (see also Fig. 2 and Fig. 5), indicating that this area is generally less prone to lateral preferential flow.

### 3.2.5 Velocities

The results of the calculated response velocities from TDR and GPR measurements are summarized in Fig. 8. The top row shows the depth distribution of observed response velocities for the entire GPR transects. The bottom row shows the TDR-based results, separated in core area profiles and the three diverging transects. Additionally to the TDR-based response velocities, GPR-based velocities observed in 0.5 m wide sections of the GPR transects which were closest to the displayed TDR profiles, are shown in the plot.



At the core area, the dominating vertical response velocity was around  $10^{-4} \text{ m s}^{-1}$ , with a tendency to increasing velocities with depth (Figure 8). As velocities were calculated for the entire soil profile above the measuring depth, this increase indicates a bypass of intermediate depths through preferential flow paths, and a limited and slow interaction with the matrix.

The highest observed vertical velocity was  $10^{-3} \text{ m s}^{-1}$  in the depth of 1.4 m below ground. The respective soil moisture signal was recorded in the very first measurement after irrigation start, which indicates that we might have even missed the first response.

Similar to the vertical velocities, the dominant TDR-based response velocity at the downhill monitoring area was in the order of magnitude of  $10^{-4} \text{ m s}^{-1}$  (Fig. 8). Response velocities of around  $10^{-3} \text{ m s}^{-1}$  were observed in six profiles all over the downhill monitoring area, of which the highest values ( $1.0$  to  $1.6 \times 10^{-3} \text{ m s}^{-1}$ , TDR4, TDR6, TDR11 and TDR17) are based on signals observed during the first profile measurements after irrigation start. The fastest response was observed in the top 0.5 m (TDR4, TDR6, and TDR10) of the soil and below a depth of 1 m (TDR6, TDR11, TDR17, and TDR18).

The GPR-based response velocities were calculated for the entire transects down to the maximum depth of approximately 4.2 m (Fig. 8 top), and for single sections close to the TDR profiles down to a depth of 1.7 m for comparison of the methods (Fig. 8 bottom). All GPR transects showed slight and localized irrigation water signals in the data collected approximately 1.5 h after irrigation start (see Fig. 6). This translates to response velocities between  $1.4 \times 10^{-3} \text{ m s}^{-1}$  to  $2.2 \times 10^{-3} \text{ m s}^{-1}$ , depending on the distance to the irrigation area and signal depth. The data of the next measurements were more explicit and suggest response velocities between  $5.4 \times 10^{-4} \text{ m s}^{-1}$  to  $8.2 \times 10^{-4} \text{ m s}^{-1}$ . Given the fact that this is a conservative estimate due to the even sparser temporal resolution in comparison to the TDR measurements, velocities are similar to or even higher than those calculated from TDR results.

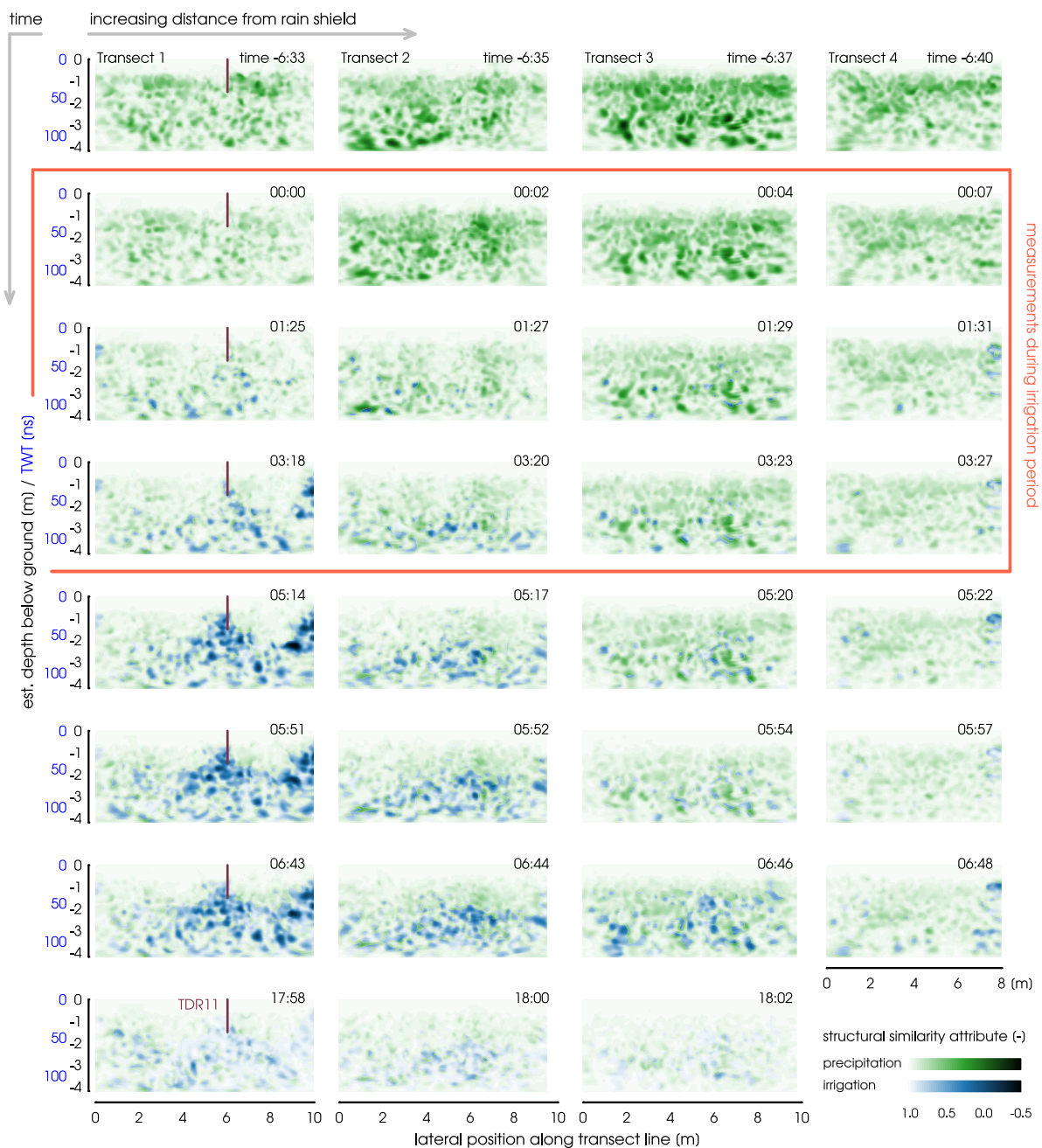


**Figure 6.** Structural similarity attributes calculated from time-lapse GPR data. All measurements were referenced to the last one 24 h after irrigation, indicating changes in the GPR reflection patterns associated with soil moisture changes. A structural similarity attribute value of 1 indicates full similarity, lower values signify higher deviation from reference state. Water from the preceding natural rain event (green) was identified by constant or increasing structural similarity attributes. Water from the experimental irrigation (blue) was identified by decreasing values after irrigation start by more than 0.15. Within one column the rows give a sequence over time (after irrigation start). Columns proceed downhill, with increasing distance from the rain shield. The purple line indicates the position and depth of TDR11.

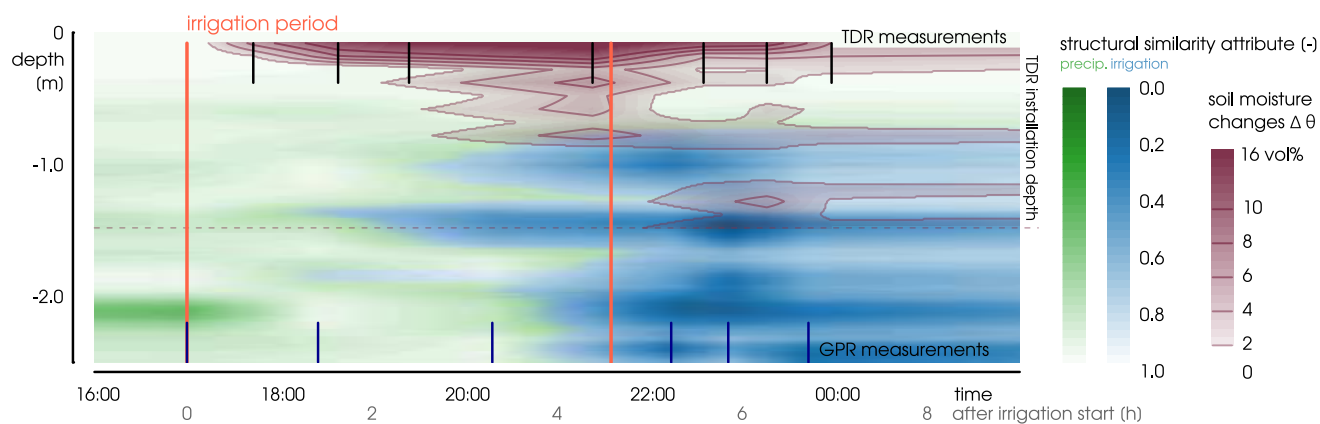


**Figure 7.** Relative soil moisture changes at TDR11 (purple) and structural similarity attribute values (green and blue) in depth over time. The signal from the natural rain event preceding the experiment is shown in green, signal attributed to irrigation water in blue. The GPR data is extracted from a narrow section of transect 1, between 6.0 m to 6.1 m in direct proximity of TDR11. The location of TDR11 is also indicated in Fig. 6. Distance between TDR11 and the depicted section of GPR transect 1 was 0.35 m. Vertical lines indicate the irrigation period (red), TDR measurements (black) and GPR measurements (blue). Data was interpolated linearly in space and time.

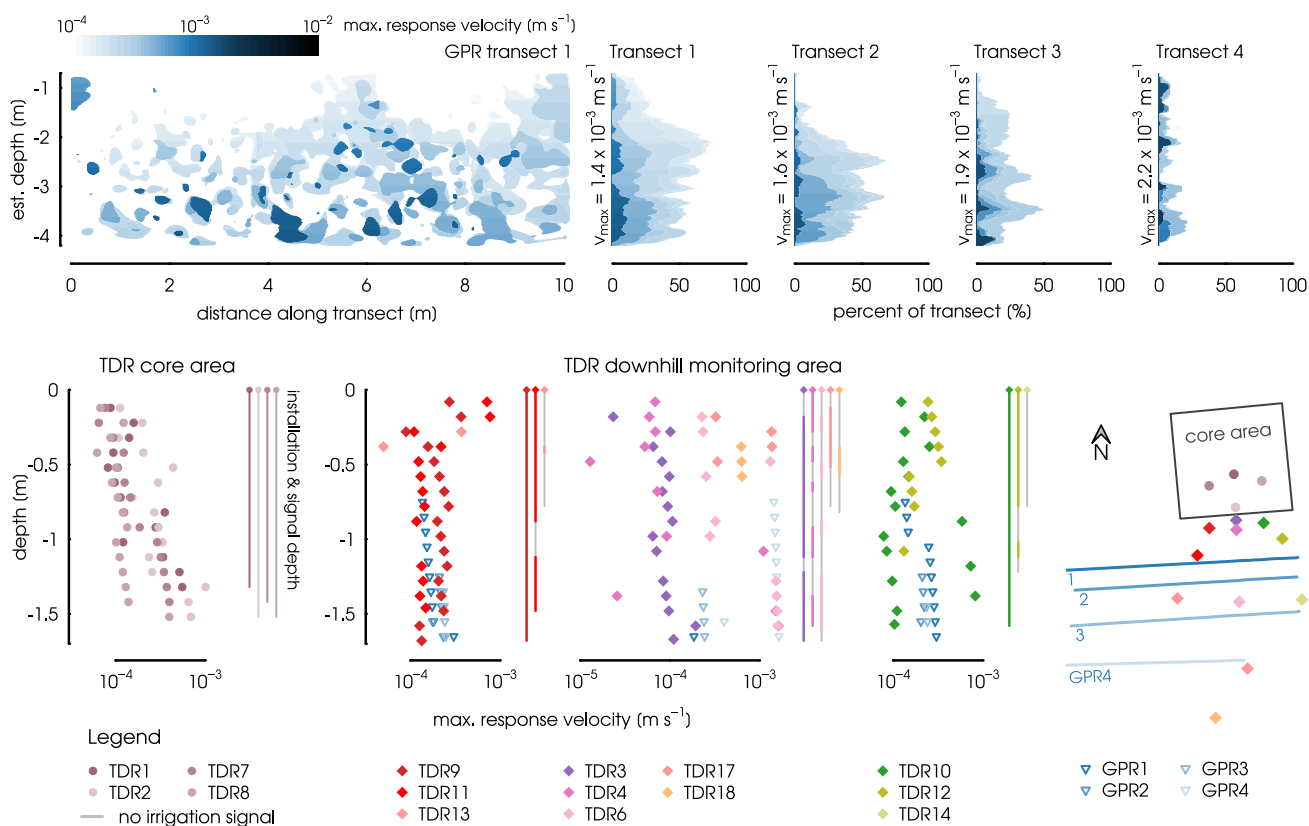


**Figure 8.** Top: Depth distributions of response velocities calculated for the four time-lapse GPR transects. The blue scale indicates the response velocity calculated from the time of first arrival for each pixel. The left plot shows the 2D results for GPR transect 1. The margin plots on the right show the same data accumulated to 1D depth profiles for all four GPR transects. Bottom: Response velocities calculated from TDR measurements at the core area (strictly vertical), and the downhill monitoring area (vertical and lateral). The three plots showing the TDR profiles at the downhill monitoring area are sorted according to the three diverging transects. Lines within the right margins of each TDR plot show the installation depths of the TDR profiles. Grey sections indicate depth increments that did not show a soil moisture signal. Additionally, GPR-based velocities derived from 0.5 m wide sections of the GPR transects close to the TDR profiles are shown.



## 4 Discussion

### 4.1 Process interpretation

#### 4.1.1 Hillslope-scale flow dynamics

The mass balance at the core area showed an overshoot in calculated mass recovery during the first 1 h of the irrigation period (Fig. 4). This might have been related to the spatial heterogeneity in irrigation intensity or lateral redistribution of water in the shallow subsurface. After that, the variability between the four profiles increased. While the storage change in TDR7 was continuous, the other three profiles showed a stepwise behavior with abrupt stagnation or even loss (TDR2) and storage increase. This behavior is interpreted as a subsequent and stepwise activation of flow paths in vertical or lateral direction. The decrease in mass recovery, which started approximately 1 h after irrigation start, signified a loss of water from the core area (0 m to 1.4 m depth). Thus, flow paths towards greater depth and the downhill monitoring area established around this time.

The fast soil moisture response in depth and at the downhill monitoring area (Fig. 5), as well as the immediate drainage after irrigation stop (Fig. 4) also suggested a high portion of mobile water. The mobile water is not bound to the matrix and likely subject to advective flow with high velocities of over  $10^{-3} \text{ m s}^{-1}$ . The order of magnitude of the velocities fitted with the *in situ* measurements of hydraulic conductivity (up to  $10^{-3} \text{ m s}^{-1}$  and higher, Jackisch et al., this issue), but clearly exceeded the potential of matrix flow for the silty matrix material. Similarly high preferential flow velocities are reported for the well studied MaiMai hillslope, with preferential flow velocities two orders of magnitude higher than matrix flow (Graham et al., 2010).

Various studies report a concentration of lateral preferential flow at a more or less impermeable bedrock interface for other sites (e.g. Graham et al., 2010; Tromp-Van Meerveld and McDonnell, 2006), which has also been hypothesized for the Colpach River catchment (e.g. Fenicia et al., 2014). However, in our irrigation experiment, both, TDR profiles and the time-lapse GPR transects revealed very heterogeneous patterns and a soil moisture response in multiple depths, as was also reported by Wienhofer et al. (2009) for a mountainous hillslope with young, structured soils.

The heterogeneous flow patterns (Fig 5 and 6) and the delayed signal in the intermediate depth at the core area (Fig 5), suggested a heterogeneous network of preferential flow paths, which bypassed a large portion of the unsaturated soil (see also Jackisch et al., this issue). At the hillslope-scale, these preferential flow paths connected and created a diffuse network of advective flow in the voids of the young skeletal soil. The structures are related to the periglacial slope deposits, which are typical for the region and landscapes which formed under similar conditions (Juilleret et al., 2011). These temporally persistent structures cover the investigated catchment and therefore, bear the potential to connect the entire hillslope, and effectively drain it as soon as the input stops.

#### 4.1.2 Catchment-scale flow dynamics

Double-peak hydrographs are likely the result of a multi-modal distribution of transit times through the catchment. They are caused by the spatial or functional organization of the landscape, which leads to the activation of different flow paths or different



source areas and storages throughout the catchment. The reasons for the occurrence of double-peak hydrographs are therefore manifold, and depend on the specific settings in the respective catchment.

The first peak of double-peak hydrographs is often attributed to saturation-excess or infiltration-excess overland flow (Burt and Butcher, 1985), or the immediate reaction of the riparian zone (e.g. Masiyandima et al., 2003), and is usually not the main focus of investigations. The reasons described for the second peak are more diverse. Lateral flow along impermeable layers or a gradual connection of previously disconnected saturated areas (Becker (2005), cited by Graeff et al. (2009)) are processes in the shallow subsurface, which have been related to double-peak hydrographs. In other catchments, water percolating deeply through fissures in the bedrock (Onda et al., 2001), overflow of a deep subsurface storage (Zillgens et al., 2007), or rapid displacement of groundwater and pressure transduction (Wenninger et al., 2004), cause the prolonged second peak.

Several studies investigated double-peak hydrographs of the Weierbach catchment and drew conclusions on their origin. Wrede et al. (2015) used dissolved silica and electrical conductivity and found that the first peak is dominated by event water, while the second peak mainly consists of pre-event water and strongly depends on antecedent conditions. Based on these observations, the first peak is attributed to fast overland flow from near-stream areas, while the second peak is attributed to subsurface flow where antecedent water is mobilized. Fenicia et al. (2014) came to a similar conclusion and identified a riparian zone reservoir as the origin of the first peak.

The stable isotope data collected during the summer storm event prior to the irrigation experiment, showed the same dynamics as observed by Wrede et al. (2015) (Fig. 3). The isotopic composition of the first peak suggested a mixture of event water and pre-event water, while the composition of the second peak indicated the dominance of pre-event water. However, in the Holtz 2 catchment, the first peak of the summer storm runoff accounted for about 4 % of the bulk precipitation amount, based on a simple water balance. This portion exceeded the existing wetland patches or riparian zones of the headwater catchment by a factor of 50, and suggests that other processes had to be involved.

Here, the timing of the GPR dynamics and the discharge response shed light on the prevailing processes. The natural rain event ended at 22:00h on June 20th, 2013. The first GPR measurements were taken at 10:00h on June 21st, approximately 12 h later (Fig. 3). Located at the lower section of the hillslope, they were interpreted to show a declining soil moisture signal, which completely disappeared 24 h after the rainfall event. Following the hypothesis of a top to bottom drainage of the hillslope, and considering the downslope location of the study site, the recorded signal represented the tailing of the shallow subsurface flow response to the natural storm event. At this time, the first peak of the hydrograph was already gone, while the second peak was on its rising limb and reached its maximum 12 h later (36 h after storm event, Fig. 3). This timing provides strong evidence that the second peak was not caused by the activation of the observed preferential flow paths.

The strong signal in the shallow subsurface (0.7 m to 4.2 m below ground), caused by the natural storm event, and the higher response despite lower intensity and duration (i.e. accumulated local input per m<sup>2</sup> at the hillslope *versus* irrigation area) in comparison to the irrigation experiment, showed that the strong signal from the natural rain event was caused by water from the entire hillslope draining through the shallow subsurface structures. The accumulated uphill area had therefore more impact on subsurface flow than the accumulated local input. This finding in combination with the high mobility of the water revealed by the irrigation experiment, suggests that the activation of preferential flow paths within subsurface structures was likely



responsible for the first immediate peak of the hydrograph, and demonstrates the importance of lateral subsurface flow at the hillslope-scale.

Connectivity established quickly within preferential flow paths, and high velocities bore the potential to route water from the hillslopes towards the river within very short time. Similarly, Van den Bos et al. (2006) stated, that the presence of preferential  
5 flow paths and steep slopes in the Colpach River catchment enable subsurface runoff, even at times when the soil and weathered zone are not yet at field capacity.

Many catchments reportedly showing double-peak hydrographs, are headwater catchments with predominately steep slopes and shallow soils, and in many cases periglacial slope deposits (Burt and Butcher, 1985; Onda et al., 2001; Graeff et al., 2009; Birkinshaw and Webb, 2010; Fenicia et al., 2014; Wrede et al., 2015). Such systems are characterized by pronounced  
10 subsurface structures and therefore, prone to heterogeneous flow patterns and preferential flow at the plot- and hillslope-scale.

The gradual activation of lateral flow paths and the resulting establishment of hillslope connectivity has also been found in other landscapes. At the Panola research catchment, bedrock topography leads to a fill-and-spill behavior (Tromp-Van Meerveld and McDonnell, 2006). In a subarctic soil filled valley (Spence and Woo, 2003), flow generation depends on the spatially variable soil storage capacity as a result of topography and the spatial heterogeneity of soil characteristics and ground  
15 frost. Flow paths within the hillslope establish and eventually connect large parts of the hillslope, causing a sudden and strong increase in subsurface flow.

The processes causing the second peak could not be resolved with the irrigation experiment, but it is hypothesized that deep percolating water from hillslopes and plateaus caused the delayed response. This hypothesis is backed by a study comparing catchments of different geology (Onda et al., 2001), where the prolonged response of double-peak hydrographs was identified  
20 as an indicator for deeply percolating subsurface flow through bedrock fissures. This theory might also apply to the here investigated catchment with its fractured schist bedrock (Kavetski et al., 2011). Furthermore, deep subsurface storage overflow (Zillgens et al., 2007) and fast groundwater displacement (Graeff et al., 2009) are processes, which possibly apply to the the Colpach River catchment. These hypotheses are also backed by the isotopic composition of the second peak, suggesting the dominance of pre-event water, and could explain the dependency of the occurrence of double-peak hydrographs on groundwater  
25 storage as described by Wrede et al. (2015).

## 4.2 Methodological discussion

### 4.2.1 General experimental setup and monitoring

Irrigation intensity and duration of the experiment were not chosen to mimic natural conditions, but to activate all potential flow paths. The limited input area and the artificial irrigation conditions both might have influenced flow patterns and processes.  
30 As such, the experimental settings might not fully allow for a direct inference of processes triggered by a natural storm event. However, the strong subsurface flow reaction to the natural storm event was generated by the accumulated input of the entire uphill area. As such, the high rates were reasonable choices to approximate the hydrological response in the shallow subsurface and could even have been stronger.



Furthermore, the sharp boundary purposely created by the rain shield, was also the advantage of this experimental design. It allowed for a separate investigation of lateral and vertical processes. Due to the separation of irrigation area and downhill monitoring area, lateral processes were easier to observe and interpret.

#### 4.2.2 Advective flow, timing and dynamics

5 The temporal proximity to the natural storm event preceding the experiment, helped to evaluate the experimental observations with regard to their transferability and their importance at the larger scale. At the same time, its impact had to be considered for data interpretation. Investigating dynamics of a system, the definition of the reference state is crucial. Natural systems are characterized by ever changing conditions and barely establish steady state in the strict sense. Even if no soil moisture changes can be observed, a uniform and continuous movement of water can not be excluded.

10 However, as we were interested in fast preferential flow, a sufficiently steady state was established when all advective momentum was dispersed. To ideally visualize the soil moisture changes caused by the advective flow, the measurements showing the least dynamics in soil moisture were chosen as the reference.

Most TDR profiles returned to approximately initial conditions after 18 h with only a marginal remaining soil moisture increase. Accordingly, the GPR signal stabilized approximately 18 h after irrigation start, showing that the fast dynamics caused by the natural rain event and the irrigation vanished. The monitoring period was thus sufficient to cover the fast response to the irrigation for both methods. The fast response to the natural rain event, in contrast, was not visible in the TDR measurements prior to the irrigation period. This discrepancy might be related to the differences in spatial coverage with regard to depth and the position along the topographic gradient. Most TDR profiles with an installation depth of more than 1 m are located uphill of GPR transect 1, where only a very weak signal of the natural rain was recorded.

#### 20 4.2.3 Monitoring methods

The installed piezometers did not show a detectable response. Neither the piezometers, nor the GPR measurements indicated a connected water table or ephemeral groundwater body at depths of less than 4 m below ground. The highly conductive preferential flow network drained the soil very effectively, even during the high input of the experimental irrigation. Saturated conditions are very improbable in such soils. Flow through adjacent structures caused some water to seep into the piezometers, but did not indicate a water table. Under such predominately unsaturated conditions, the piezometer response is very sensitive to their specific location. This observation shows that piezometers are not well suited for the observation of hydrological processes in highly structured and well drained soils.

GPR measurements are influenced by a variety of factors, such as repositioning accuracy, antenna coupling and inaccuracies in the data recording and processing. Therefore, special care was taken about exact positioning of the GPR antennas, by using an automated tracking station and wooden guides for exact positioning. While soil properties other than soil moisture were assumed stable over the course of the experiment, methodological factors, such as surface contact of the antennas and signal deviation below areas of large differences in radar velocity are presumably the only additional source of artifacts in the recorded radargrams.



While we deem the GPR signals to be reliable indicators for soil moisture changes, care has to be taken not to over-interpret the resulting data. Firstly, the structural similarity attribute is not linearly dependent on soil moisture changes. This fact, in combination with the depth attribution based on a constant GPR wave velocity, suggests that GPR images are to be interpreted as a qualitative map of changes rather than a tool to precisely locate and quantify preferential flow paths. Secondly, structural similarity attributes highlight relative changes, without specifying the direction of the change. Our interpretation that decreasing similarity indicates increasing soil moisture, is based on the assumption that the reference measurement was the driest.

However, we observed a fast and consistent evolution of the GPR patterns over time. Furthermore, the good temporal and spatial correspondence with TDR measurements also provides strong evidence that the observed signal is actually related to soil moisture changes. Taking all the above mentioned aspects into account, the GPR data provides valuable insight into subsurface flow processes, which is hard to obtain with other methods.

While soil moisture is a commonly used indicator for flow processes in the unsaturated zone, its measurement is difficult. Our challenge was to record full profiles as continuously as possible. The applied technique allowed for that and yielded a decent data set. However, besides the positioning of the probes and the limited temporal resolution implied by the measuring routine, the concept of soil moisture measurement itself exerts some limitations. The penetration depth of the TDR signal is subject to change with soil moisture. As such the absolute values may be largely ambiguous in terms of precise determination of the amount of water. Furthermore, the scale discrepancy between integration volume and flow path volume constrains the sensitivity to high velocities in small-scale flow paths, which will be discussed in Sec. 4.2.5.

#### 4.2.4 Combination of monitoring methods

Soil moisture measurements at the core area disclosed a gradual wetting of the top 0.4 m of the soil. This could mistakenly be interpreted as a continuous wetting front and described as vertical matrix flow based on 1D assumptions. The information on spatial patterns and flow processes obtained from measurements in greater depths and GPR transects, however, revealed that this simplification is not adequate to properly represent all processes.

Furthermore, a separate interpretation of single TDR profiles or even each of the three TDR transects (Fig. 2) on its own would have led to different conclusions about subsurface flow processes. The characteristics and extent of flow patterns and dynamics could only be inferred from the combination of a dense soil moisture monitoring network and the time-lapse GPR transects. A limited number of point observations would have been very likely to either miss hydrologically active structures or to overestimate their impact. The two dimensional monitoring put single measurements into spatial context and revealed the process scale and adequate observation density needed for a realistic representation of the investigated processes.

In contrast to conventional trenches or point measurements, the presented combination of TDR profiles and 2D time-lapse GPR measurements provides the spatial context that is crucial for the investigation of complex preferential flow networks. In contrast to dye tracer excavations, time-lapse GPR measurements yield the temporal component, which is necessary to cover the highly dynamic processes. This combination of methods allows for repetitions in time and space and avoids the manipulating effect of a trench face on unsaturated flow paths (Atkinson, 1978). In recent years, the combination of TDR and electric resistivity tomography (ERT) was successfully applied to monitor soil moisture dynamics at the hillslope-scale



(Wenninger et al., 2008; Garré et al., 2013; Hübner et al., 2014). Long measurement times and a limitation in electrode spacing, however, lead to a comparably low spatial and temporal resolution. Under the given circumstances and research questions, GPR measurements are less restricted in resolution and are therefore better suited for the observation of fast and small-scale preferential flow.

#### 5 4.2.5 Integration volume and resolution and scale

With a measurement principle based on the dielectric permittivity, TDR and GPR both take snapshots in time and describe the current state of the subsurface. The momentum of the water is not measured directly, and water fluxes are inferred indirectly from changes in soil moisture and reflection patterns. Response velocities can only be derived from the spatial and temporal dynamics of soil moisture, and the separation of diffusive and advective movement is difficult.

10 While a vertically proceeding wetting front is relatively easy to observe and quantify by means of a 1D soil moisture profile, the identification and investigation of preferential flow paths is more difficult. Preferential flow paths are spatially and temporally discrete and in the case of the investigated hillslope expected to be smaller than the integration volume of both GPR and TDR. Thus, preferential flow paths will only become visible if their volume is comparably large, or if they interact with the surrounding matrix and increase the overall soil moisture. Diffusive flow has better visibility and its importance is thus likely  
15 to be overestimated. Fraction and velocity of advective flow are likely underestimated due to their low or delayed soil moisture footprint.

The dynamics of preferential flow is often characterized by a stepwise activation of single flow paths. Temporal interpolation between measurements is therefore not appropriate. The measurement frequency directly impairs the resolution and detectable maximum velocity. The 2 vol% threshold applied to identify the first response in soil moisture during this experiment is rather  
20 high. We cannot exclude that the actual first response happens earlier without being detected. Furthermore, several locations already showed a soil moisture response in the very first measurement after irrigation start. Figure 8 shows that the setup of the GPR measurements was not capable of capturing response velocities faster than  $2.2 \times 10^{-3} \text{ m s}^{-1}$ . The calculated velocities from both, GPR and TDR measurements, are therefore rough estimates and likely to underestimate preferential flow velocities. To reliably quantify maximum response velocities, a higher measurement frequency would have been necessary.

25 The size of the integration volume is a trade-off between representativity and sensitivity, and the ideal integration volume strongly depends on the research objective. While a small integration volume is able to instantly detect small preferential flow paths as they establish, it requires a higher number of spatial repetitions to be representative for the investigated system. 2D transects, as provided by the time-lapse GPR measurements, are a good improvement over point observations and 1D profiles. Nevertheless, the resulting patterns can only be properly interpreted if the characteristics and scale of preferential flow paths  
30 are known.

#### 4.2.6 Multi-scale approach

The experimental investigation of the runoff generation, and especially the origin of double-peak hydrographs, usually focuses on integrated signals such as environmental tracers (Zillgens et al., 2007; Wrede et al., 2015) and water balance calculations.



While many studies use models to prove or reject different hypothesis (Graeff et al., 2009; Fenicia et al., 2014), the direct observations of subsurface flow processes in relation with double-peak hydrographs are sparse. Piezometers (Masiyandima et al., 2003) are restricted to processes in the saturated zone. Distributed soil moisture measurements or temperature profiles (Birkinshaw and Webb, 2010) are based on the assumption of continuous processes and often neglect lateral flow processes.

5 The combined investigation of hillslope-scale processes and catchment-scale dynamics allows for conclusions on the relation between subsurface flow and runoff behavior.

Jackisch et al. (this issue) complement the hillslope-scale irrigation experiment with a structural survey as well as plot-scale samples and dye tracer experiments, to improve our understanding of small-scale processes and their dependency on subsurface structures. These two studies combine to a multi-scale perspective on preferential flow processes and the controlling structures.



## 5 Conclusions

The study site is an example for headwater catchments with steep slopes and young and highly structured soils, deemed representative for landscapes that formed under similar conditions. Here, preferential flow paths quickly develop in the unsaturated zone within minutes after a rain event, causing fast establishment of hillslope-scale connectivity. In combination with the high response velocities of up to  $10^{-3} \text{ ms}^{-1}$  or faster, and the large portion of mobile water, these flow paths have the potential to route a large amount of water from the hillslopes towards the stream. The observed processes, thus, control the transit-time distribution of the catchment and impact its overall runoff behavior.

The strong dynamics and high spatial variability of preferential flow challenge the investigation of these processes. While we were able to describe the overall flow dynamics, the spatio-temporal resolution of our monitoring setup was not sufficient to reliably quantify the maximum response velocities. Our study has furthermore shown that causality and importance of observations can only be evaluated if the necessary context is known. This context includes knowledge on the spatio-temporal patterns on the one hand, and relevant process scales on the other.

The spatio-temporal context is provided by a combination of quantitative point measurements (TDR), qualitative mapping of patterns and dynamics (2D time-lapse GPR) and the observation of integrated system response (hydrographs and staple isotopes). Either of these approaches provides a substantial piece to the puzzle, while neither of them on its own would have provided the full picture. The experiment has shown that time-lapse GPR measurements are a powerful tool which provides new perspectives for the investigation of preferential flow processes in hillslopes. The methodology's flexibility and minimally invasive character allow for repetitions in time and space, and thus, the direct observation of processes under driven conditions. This provides perspectives which can barely be achieved with other approaches.

The combination of catchment-scale dynamics and hillslope-scale processes allows us to infer the overall functioning of the catchment. However, while these processes and dynamics could well be observed with the presented approach, there is a lack of process understanding at the smaller scale. Even though the experiment gave us a good idea of the general dynamics and patterns of the relevant processes, the applied resolution was not sufficient to reliably determine maximum velocities and describe discrete spatial properties of the preferential flow paths. Especially the link between processes and structures is still missing, as the relevant process scale is below the resolution of the applied methods.

The second part of this study presented by Jackisch et al. (this issue) focuses on this missing link by complementing the hillslope-scale irrigation experiment with plot-scale dye tracer experiments and structural exploration. The synthesis of the results from both parts provides detailed insights into hillslope processes and preferential flow.



*Acknowledgements.* We are grateful to Marcel Delock, Lisei Köhn and Marvin Reich for their support during fieldwork, as well as Markus Morgner and Jean Francois Iffly for technical support, Britta Kattenstroth for hydrometeorological data acquisition and isotope sampling and Barbara Herbstritt and Begoña Lorente Sistiaga for laboratory work. Laurent Pfister and Jean-Francois Iffly from the Luxembourg Institute of Science and Technology (LIST) are acknowledged for organizing the permissions for the experiments and providing discharge data for 5 Weierbach 1 and Colpach. This study is part of the DFG funded CAOS project 'From Catchments as Organised Systems to Models based on Dynamic Functional Units' (FOR 1598).



## References

- Allroggen, N. and Tronicke, J.: Attribute-based analysis of time-lapse ground-penetrating radar data, *Geophysics*, 81, H1–H8, 2015.
- Allroggen, N., Tronicke, J., Delock, M., and Böniger, U.: Topographic migration of 2D and 3D ground-penetrating radar data considering variable velocities, *Near Surface Geophysics*, 13, 253–259, doi:10.3997/1873-0604.2014037, 2015a.
- 5 Allroggen, N., van Schaik, L., and Tronicke, J.: 4D ground-penetrating radar during a plot scale dye tracer experiment, *Journal of Applied Geophysics*, 118, 139–144, doi:10.1016/j.jappgeo.2015.04.016, 2015b.
- Anderson, A. E., Weiler, M., Alila, Y., and Hudson, R. O.: Dye staining and excavation of a lateral preferential flow network, *Hydrology and Earth System Sciences Discussions*, 5, 1043–1065, 2008.
- Atkinson, T.: Techniques for measuring subsurface flow on hillslopes, *Hillslope Hydrology*, pp. 73–120, 1978.
- 10 Bachmair, S. and Weiler, M.: Hillslope characteristics as controls of subsurface flow variability, *Hydrology and Earth System Sciences*, 16, 3699–3715, doi:10.5194/hess-16-3699-2012, 2012.
- Bachmair, S. and Weiler, M.: Interactions and connectivity between runoff generation processes of different spatial scales, *Hydrological Processes*, 28, 1916–1930, doi:10.1002/hyp.9705, 2014.
- Beven, K. and Germann, P.: Macropores and water flow in soils, *Water Resources Research*, 18, 1311–1325, 1982.
- 15 Beven, K. and Germann, P.: Macropores and water flow in soils revisited, *Water Resources Research*, 49, 3071–3092, doi:10.1002/wrcr.20156, 2013.
- Birken, R. and Versteeg, R.: Use of four-dimensional ground penetrating radar and advanced visualization methods to determine subsurface fluid migration, *Journal of Applied Geophysics*, 43, 215–226, 2000.
- Birkinshaw, S. J. and Webb, B.: Flow pathways in the Slapton Wood catchment using temperature as a tracer, *Journal of Hydrology*, 383, 269–279, doi:10.1016/j.jhydrol.2009.12.042, 2010.
- 20 Blume, T. and van Meerveld, H. I.: From hillslope to stream: methods to investigate subsurface connectivity, *Wiley Interdisciplinary Reviews: Water*, 2, 177–198, doi:10.1002/wat2.1071, 2015.
- Boeniger, U. and Tronicke, J.: On the Potential of Kinematic GPR Surveying Using a Self-Tracking Total Station: Evaluating System Crosstalk and Latency, *IEEE Transactions on Geoscience and Remote Sensing*, 48, 3792–3798, doi:10.1109/TGRS.2010.2048332, 2010.
- 25 Bradford, J. H., Harper, J. T., and Brown, J.: Complex dielectric permittivity measurements from ground-penetrating radar data to estimate snow liquid water content in the pendular regime, *Water Resources Research*, 45, 1–12, doi:10.1029/2008WR007341, 2009.
- Burt, T. and Butcher, D.: Topographic controls of soil moisture distributions, *Journal of Soil Science*, 36, 469–486, 1985.
- Colbach, R. and Maquil, R.: Carte géologique du Luxembourg 1:25000-Feuille n° 7 Rédange, Service Géologique du Luxembourg, Luxembourg, 2003.
- 30 Fenicia, F., Kavetski, D., Savenije, H. H. G., Clark, M. P., Schoups, G., Pfister, L., and Freer, J.: Catchment properties, function, and conceptual model representation: is there a correspondence?, *Hydrological Processes*, 28, 2451–2467, doi:10.1002/hyp.9726, 2014.
- Flury, M., Flühler, H., Jury, W. A., and Leuenberger, J.: Susceptibility of soils to preferential flow of water: a field study, *Water Resources Research*, 30, 1945–1954, 1994.
- Garré, S., Coteur, I., Wonglecharoen, C., Kongkaew, T., Diels, J., and Vanderborght, J.: Noninvasive Monitoring of Soil Water Dynamics in Mixed Cropping Systems: A Case Study in Ratchaburi Province, Thailand, *Vadose Zone Journal*, 12, –, doi:10.2136/vzj2012.0129, 2013.
- 35 Gazis, C. and Feng, X.: A stable isotope study of soil water: evidence for mixing and preferential flow paths, *Geoderma*, 119, 97–111, doi:10.1016/S0016-7061(03)00243-X, 2004.



- Gerke, H. H.: Preferential flow descriptions for structured soils, *Journal of Plant Nutrition and Soil Science*, 169, 382–400, doi:10.1002/jpln.200521955, 2006.
- Gerke, H. H., Germann, P., and Nieber, J.: Preferential and Unstable Flow: From the Pore to the Catchment Scale, *Vadose Zone Journal*, 9, 207, doi:10.2136/vzj2010.0059, 2010.
- 5 Germann, P. F.: *Preferential Flow*, Geographica Bernensia, Institute of Geography, University of Bern, Bern, 2014.
- Graeff, T., Zehe, E., Reusser, D., Lück, E., Schröder, B., Wenk, G., John, H., and Bronstert, A.: Process identification through rejection of model structures in a mid-mountainous rural catchment: observations of rainfall–runoff response, geophysical conditions and model inter-comparison, *Hydrological Processes*, 23, 702–718, doi:10.1002/hyp.7171, 2009.
- Graham, C. B., Woods, R. A., and McDonnell, J. J.: Hillslope threshold response to rainfall: (1) A field based forensic approach, *Journal of Hydrology*, 393, 65–76, doi:10.1016/j.jhydrol.2009.12.015, 2010.
- 10 Guo, L., Chen, J., and Lin, H.: Subsurface lateral preferential flow network revealed by time-lapse ground-penetrating radar in a hillslope, *WATER RESOURCES RESEARCH*, 50, 9127–9147, doi:10.1002/2013WR014603, 2014.
- Haarder, E. B., Looms, M. C., Jensen, K. H., and Nielsen, L.: Visualizing Unsaturated Flow Phenomena Using High-Resolution Reflection Ground Penetrating Radar, *Vadose Zone Journal*, 10, 84–97, doi:10.2136/vzj2009.0188, 2011.
- 15 Hincapié, I. and Germann, P.: Water content wave approach applied to neutron radiographs of finger flow, *Vadose Zone Journal*, 9, 278–284, doi:10.2136/vzj2009.0102, 2010.
- Hübner, R., Heller, K., Günther, T., and Kleber, a.: Monitoring hillslope moisture dynamics with surface ERT and hydrometric point measurement: a case study from Ore Mountains, Germany, *Hydrology and Earth System Sciences Discussions*, 11, 5859–5903, doi:10.5194/hessd-11-5859-2014, 2014.
- 20 IUSS Working Group WRB: World reference base for soil resources, *World Soil Resources Report*, 103, 2006.
- Jackisch, C., Angermann, L., Allroggen, N., Sprenger, M., Tronicke, J., Weiler, M., Blume, T., and Zehe, E.: *In situ* investigation of rapid subsurface flow: Identification of relevant spatial structures beyond heterogeneity, *Hydrology and Earth System Sciences*, this issue.
- Jol, H. M., ed.: *Ground penetrating radar theory and applications*, Elsevier Science, Amsterdam, 1 edn., 2009.
- Juillet, J., Iffly, J., Pfister, L., and Hissler, C.: Remarkable Pleistocene periglacial slope deposits in Luxembourg (Oesling): pedological implication and geosite potential, *Bulletin de la Société des Naturalistes Luxembourgeois*, 112, 125–130, 2011.
- 25 Kavetski, D., Fenicia, F., and Clark, M. P.: Impact of temporal data resolution on parameter inference and model identification in conceptual hydrological modeling: Insights from an experimental catchment, *Water Resources Research*, 47, doi:10.1029/2010WR009525, 2011.
- Köhne, J. M., Köhne, S., and Šimůnek, J.: A review of model applications for structured soils: a) Water flow and tracer transport, *Journal of Contaminant Hydrology*, 104, 4–35, doi:10.1016/j.jconhyd.2008.10.002, 2009.
- 30 Lambot, S., Binley, A., Slob, E., and Hubbard, S.: Ground Penetrating Radar in Hydrogeophysics, *Vadose Zone Journal*, 7, 137, doi:10.2136/vzj2007.0180, 2008.
- Leibundgut, C., Maloszewski, P., and Külls, C.: *Tracers in hydrology*, John Wiley & Sons, 2011.
- Masiyandima, M. C., van de Giesen, N., Diatta, S., Windmeijer, P. N., and Steenhuis, T. S.: The hydrology of inland valleys in the sub-humid zone of West Africa: rainfall-runoff processes in the M'bé experimental watershed, *Hydrological Processes*, 17, 1213–1225, doi:10.1002/hyp.1191, 2003.
- 35 McGlynn, B. L., McDonnell, J. J., and Brammer, D. D.: A review of the evolving perceptual model of hillslope flowpaths at the Maimai catchments, New Zealand, *Journal of Hydrology*, 257, 1–26, 2002.



- McGuire, K. J. and McDonnell, J. J.: Hydrological connectivity of hillslopes and streams: Characteristic time scales and nonlinearities, *Water Resources Research*, 46, n/a–n/a, doi:10.1029/2010WR009341, 2010.
- Onda, Y., Komatsu, Y., Tsujimura, M., and Fujihara, J. I.: The role of subsurface runoff through bedrock on storm flow generation, *Hydrological Processes*, 15, 1693–1706, doi:10.1002/hyp.234, 2001.
- 5 Pearce, A. J., Stewart, M. K., and Sklash, M. G.: Storm runoff generation in humid headwater catchments: 1. Where does the water come from?, *Water Resources Research*, 22, 1263–1272, 1986.
- Peralta-Tapia, A., Sponseller, R. A., Tetzlaff, D., Soulsby, C., and Laudon, H.: Connecting precipitation inputs and soil flow pathways to stream water in contrasting boreal catchments, *Hydrological Processes*, 29, 3546–3555, doi:10.1002/hyp.10300, 2014.
- Schmelzbach, C., Tronicke, J., and Dietrich, P.: Three-dimensional hydrostratigraphic models from ground-penetrating radar and direct-push  
10 data, *Journal of Hydrology*, 398, 235–245, 2011.
- Schmelzbach, C., Tronicke, J., and Dietrich, P.: High-resolution water content estimation from surface-based ground-penetrating radar reflection data by impedance inversion, *Water Resources Research*, 48, 2012.
- Sheng, F., Liu, H., Wang, K., Zhang, R., and Tang, Z.: Investigation into preferential flow in natural unsaturated soils with field multiple-tracer infiltration experiments and the active region model, *Journal of Hydrology*, 508, 137–146, doi:10.1016/j.jhydrol.2013.10.048, 2014.
- 15 Snehota, M., Jelinkova, V., Sacha, J., Frycova, M., Cislerova, M., Vontobel, P., and Hovind, J.: Experimental Investigation of Preferential Flow in a Near-saturated Intact Soil Sample, *Physics Procedia*, 69, 496–502, doi:10.1016/j.phpro.2015.07.070, 2015.
- Spence, C. and Woo, M.-k.: Hydrology of subarctic Canadian shield: soil-filled valleys, *Journal of Hydrology*, 279, 151–166, doi:10.1016/S0022-1694(03)00175-6, 2003.
- Steelman, C. M., Endres, A. L., and Jones, J. P.: High-resolution ground-penetrating radar monitoring of soil moisture dynamics: Field  
20 results, interpretation, and comparison with unsaturated flow model, *Water Resources Research*, 48, 1–17, doi:10.1029/2011WR011414, 2012.
- Trinks, I., Stümpel, H., and Wachsmuth, D.: Monitoring water flow in the unsaturated zone using georadar, *First Break*, 19, 679–684, 2001.
- Tromp-Van Meerveld, H. J. and McDonnell, J. J.: Threshold relations in subsurface stormflow: 2. The fill and spill hypothesis, *Water Resources Research*, 42, 1–11, doi:10.1029/2004WR003800, 2006.
- 25 Truss, S., Grasmueck, M., Vega, S., and Viggiano, D. A.: Imaging rainfall drainage within the Miami oolitic limestone using high-resolution time-lapse ground-penetrating radar, *Water Resources Research*, 43, W03405, doi:10.1029/2005WR004395, 2007.
- Uhlenbrook, S.: Catchment hydrology – a science in which all processes are preferential, *Hydrological Processes*, 20, 3581–3585, doi:10.1002/hyp.6564, 2006.
- Van den Bos, R., Hoffmann, L., Juilleret, J., Matgen, P., and Pfister, L.: Regional runoff prediction through aggregation of first-order hydro-  
30 logical process knowledge: a case study, *Hydrological Sciences Journal*, 51, 1021–1038, doi:10.1623/hysj.51.6.1021, 2006.
- Van Schaik, L., Palm, J., Klaus, J., Zehe, E., and Schröder, B.: Linking spatial earthworm distribution to macropore numbers and hydrological effectiveness, *Ecohydrology*, 7, 401–408, doi:10.1002/eco.1358, 2014.
- Vogel, T., Sanda, M., Dusek, J., Dohnal, M., and Votrubova, J.: Using Oxygen-18 to Study the Role of Preferential Flow in the Formation of Hillslope Runoff, *Vadose Zone Journal*, 9, 252–259, doi:10.2136/vzj2009.0066, 2010.
- 35 Šimůnek, J., Jarvis, N. J., van Genuchten, M. T., and Gardenas, A.: Review and comparison of models for describing non-equilibrium and preferential flow and transport in the vadose zone, *Journal of Hydrology*, 272, 14–35, doi:10.1016/S0022-1694(02)00252-4, 2003.
- Wang, Z., Bovik, A. C., Sheikh, H. R., and Simoncelli, E. P.: Image quality assessment: from error visibility to structural similarity, *IEEE Transactions on Image Processing*, 13, 600–612, 2004.



- Weiler, M. and McDonnell, J. J.: Conceptualizing lateral preferential flow and flow networks and simulating the effects on gauged and ungauged hillslopes, *Water Resources Research*, 43, 1–13, doi:10.1029/2006WR004867, 2007.
- Wenninger, J., Uhlenbrook, S., Tilch, N., and Leibundgut, C.: Experimental evidence of fast groundwater responses in a hillslope/floodplain area in the Black Forest Mountains, Germany, *Hydrological Processes*, 18, 3305–3322, doi:10.1002/hyp.5686, 2004.
- 5 Wenninger, J., Uhlenbrook, S., Lorentz, S., and Leibundgut, C.: Identification of runoff generation processes using combined hydrometric, tracer and geophysical methods in a headwater catchment in South Africa, *Hydrological Sciences Journal*, 53, 65–80, 2008.
- Wienhofer, J., Germer, K., Lindenmaier, F., Färber, A., and Zehe, E.: Applied tracers for the observation of subsurface stormflow at the hillslope scale, *Hydrology and Earth System Sciences*, 13, 2961–3006, 2009.
- Wrede, S., Fénicia, F., Martínez-Carreras, N., Juilleret, J., Hissler, C., Krein, A., Savenije, H. H. G., Uhlenbrook, S., Kavetski, D., and Pfister,  
10 L.: Towards more systematic perceptual model development: a case study using 3 Luxembourgish catchments, *Hydrological Processes*, 29, 2731–2750, doi:10.1002/hyp.10393, 2015.
- Zehe, E., Blume, T., and Blöschl, G.: The principle of ‘maximum energy dissipation’: a novel thermodynamic perspective on rapid water flow in connected soil structures, *Philosophical Transactions of the Royal Society B: Biological Sciences*, 365, 1377–1386, 2010.
- Zehe, E., Ehret, U., Pfister, L., Blume, T., Schröder, B., Westhoff, M., Jackisch, C., Schymanski, S. J., Weiler, M., Schulz, K., Allroggen,  
15 N., Tronicke, J., Dietrich, P., Scherer, U., Eccard, J., Wulfmeyer, V., and Kleidon, A.: Functional units: a novel framework to explore the link between spatial organization and hydrological functioning of intermediate scale catchments, *Hydrology and Earth System Sciences Discussions*, 11, 3249–3313, doi:10.5194/hessd-11-3249-2014, <http://www.hydrol-earth-syst-sci-discuss.net/11/3249/2014/>, 2014.
- Zhao, P., Tang, X., Zhao, P., Wang, C., and Tang, J.: Tracing water flow from sloping farmland to streams using oxygen-18 isotope to study a small agricultural catchment in southwest China, *Soil and Tillage Research*, 134, 180–194, doi:10.1016/j.still.2013.08.005, 2013.
- 20 Zillgens, B., Merz, B., Kimbauer, R., and Tilch, N.: Analysis of the runoff response of an alpine catchment at different scales, *Hydrology and Earth System Sciences*, 11, 1441–1454, 2007.